Article

INTERNATIONAL JOURNAL OF DAMAGE MECHANICS

International Journal of Damage Mechanics
2018, Vol. 27(9) 1291–1306

DOI: 10.1177/1056789517704029
journals.sagepub.com/home/ijd
SAGE

Assessment of ductile failure models in single-pass wire drawing processes

Alvaro A González[1], Diego J Celentano[2] and Marcela A Cruchaga[1]

Abstract

The present work reports a comparative study of ductile failure models applied to an Al-2011 aluminum alloy single-pass wire drawing process using different reductions. The material damage experienced in the wire after passing through the die is evaluated using the well-known Rice and Tracey, Cockcroft and Latham, Brozzo and Modified Chaouadi models. Due to the fact that nonrealistic damage predictions are found for the highest studied wire reduction, an alternative uncoupled failure criterion combining the effect of deformation and triaxility is proposed. The ability of these five models in predicting the formation of chevrons in the process is the main focus of this research. First, the model parameters are characterized by means of numerical simulations of the tensile test. Then, the predictions of the numerical analyses of the drawing process are compared with available experimental results where physical evidence of chevrons was found. Relevant variables are analyzed to determine their incidence in the formation of central bursts. Finally, the performance of this new model is assessed for the full reduction scenarios.

Keywords

Wire drawing, ductile fracture, damage, chevron formation, central bursting

Introduction

In the metal-mechanical industry, wire production is carried out by means of the well-known plastic forming process called drawing, which reduces the cross-section of the material by pulling it through a rigid die to induce plastic deformations in the material. This process takes place either in one step (single-pass) or in several steps (multi-pass). Wire drawing is mainly characterized geometrically by the input diameter (d_i) and the output diameter (d_o), giving rise to the total reduction achieved at each drawing die ($1-(d_o/d_i)^2$). Moreover, each die has a characteristic angle (α). A schematic view of

[1]Departamento de Ingeniería Mecánica, Universidad de Santiago de Chile (USACH), Chile
[2]Departamento de Ingeniería Mecánica y Metalúrgica, Pontificia Universidad Católica de Chile, Chile

Corresponding author:
Diego J Celentano, Pontificia Universidad Católica de Chile, Av. Vicuña Mackenna 4860, Santiago de Chile, 7820436, Chile.
Email: dcelentano@ing.puc.cl

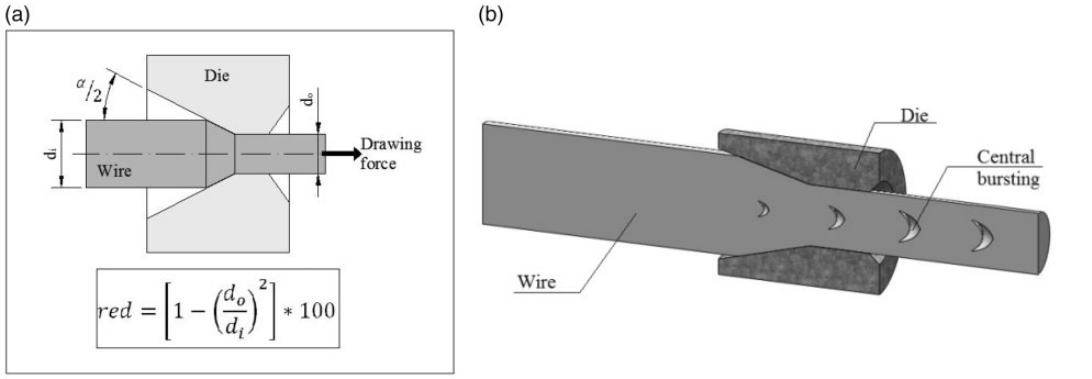

Figure 1. Schematic representation of the wire drawing process (a) and central bursting (b).

the process is shown in Figure 1(a). During this process, it is possible to find faults that start within the material and can only be seen when the drawn wire breaks. In such a case, the process must be stopped, and the material must be threaded again through the drawing die. Figure 1(b) shows this kind of fault known as ''central burst'' or ''chevron'' that corresponds to a ductile fracture (Avitzur, 1983). Ductile fracture is found to be the result of nucleation, growth, and later coalescence of microcavities in the material and, it is characterized macroscopically by showing high plastic deformation levels and low propagation speed of the crack. Furthermore, higher deformation energy levels are needed than in the case of fragile fracture.

Different fracture models have been proposed to date, distinguishing between those in which the damage level does not affect the stress–strain relationship (uncoupled models) and those that incorporate a parameter that quantifies the degradation of the material subjected to stresses in its constitutive equations (coupled models). The pioneering works related to ductile damage prediction were proposed by Freudenthal (1950) and McClintock (1968) (uncoupled models), and Gurson (1977) and Lemaitre (1985) (coupled models). Since the present work is focused on the performance assessment of different uncoupled models, relevant developments within this framework are briefly presented below.

One of the first uncoupled models proposed for predicting the start of ductile fracture was presented by Freudenthal (1950). It is known as the total plastic work criterion, stating that the critical parameter in a forming process is given by the absorbed plastic energy. Once that value is exceeded, the fracture process starts. Later, McClintock (1968) presented an expression that quantifies the growth of an elliptical void subjected to a triaxial tension field with a fixed orientation. The critical parameter defined in this model depends on the principal stresses defined at the major and minor axes of the ellipse, and it also depends on the hardening exponent obtained from the constitutive law. This model was used by Sowerby et al. (1985) to assess the damage and its accumulation in AISI 1045 steel samples subjected to different compression tests, showing that it approaches properly the growth of microvoids, but it does not account for the phenomenon of nucleation and later coalescence. Moreover, Rice and Tracey (1969) proposed a variational principle for the growth of cavities in a rigid plastic material that contains an initially spherical internal microvoid that is subjected to a remote deformation velocity field. The proposed principle is applied to different stresses with the purpose of getting a good relation that determines the behavior and the evolution of the microvoid. Finally, they proposed a criterion that considers the influence of the triaxiality of the stress field on the evolution of the cavity. The critical void radius is obtained when the rupture deformation is

reached, determining the onset of the material fracture process. Furthermore, the proposed criterion by Cockcroft and Latham (1968) considered that the ductile fracture is based on the principal stress work whose critical value is obtained from a characterization of the material by means of an uniaxial stress test. This model, together with the total plastic work model developed by Freudenthal, was used by Choi et al. (2010) to numerically simulate the formation of central bursts and their later evolution in an extrusion process. Comparing both models, it was determined that the Freudenthal model induced the formation of an external crack (in the wire-die contact zone), while the Cockcroft and Latham model led to central bursting with a good agreement with respect to the data reported experimentally in relation to the distance between the chevrons where, in addition, it was also determined that the size of the mesh discretization used in the finite element analysis affects directly the formation and evolution of the central bursts. The criterion defined by Brozzo et al. (1972) proposes an empirical modification of the Cockcroft and Latham criterion, taking into account the effect of the hydrostatic pressure in the ductile fracture prediction. This is one of the models with which Komori (2003) was able to reproduce numerically the formation of chevrons in a copper wire drawing, a multi-pass process. A more detailed description of the formulation proposed by each of the uncoupled models described above can be found in the work developed by Ran and Fu (2016).

Chaouadi et al. (1994) proposed a model assuming that during the plastification the damage develops in the material through the growth of cavities according to a plastic work criterion. This model was used by McAllen and Phelan (2005), who incorporated a modification based on the proposal by Huang (1991) where the growth of voids for different levels of triaxiality was assessed. Then, Pardoen et al. (1996) reevaluated the expression proposed by Rice and Tracey, and the new values obtained were used into the Chaouadi model. This modified version was used by McAllen and Phelan (2007), reproducing well the formation of chevrons in the wire drawing process, both in single and multi-pass stages.

Several studies have been developed to date focusing on the central bursting initiation in both wire drawing and extrusion processes using different materials (e.g. cooper, aluminum, steel). They are briefly summarized in Table 1. Most of them use the Cockcroft and Latham ductile fracture criterion, which only consider the maximum principal stress and does not take into account the effect

Table 1. Studies on the central bursting initiation in both wire drawing and extrusion processes.

Author	Used models	Applications	Material	Analysis
Ko et al. (2000)	Cockcroft and Latham	Extrusion and wire drawing	Aluminum	Experimental and numerical
Komori (2003)	Oyane, Cockcroft and Latham, Brozzo, Freudenthal	Wire drawing	Cooper	Experimental and numerical
McAllen and Phelan (2007)	Chaouadi	Wire drawing	Aluminium	Numerical
Norasethasopon et al. (2008)	Cockcroft and Latham	Wire drawing	Cooper	Numerical
Choi et al. (2010)	Cockcroft and Latham	Extrusion	Aluminum and steel alloys	Numerical
Haddi et al. (2012)	Cockcroft and Latham	Wire drawing	Cooper	Experimental and numerical

of the relation between the hydrostatic pressure and von Misses stress. Moreover, few studies have been done to relate triaxiality with fracture initiation conditions. It is well known that an increase in reductions generates considerable variation in the hydrostatic pressure and, therefore, this fact justifies the use of models that incorporate this parameter (e.g. Rice and Tracey or Chaouadi models).

In this work, a comparative study of ductile failure models applied to an Al-2011 aluminum alloy single-pass wire drawing process using different reductions is presented. This process is numerically simulated in the context of the finite element method where the material damage is evaluated using the Rice and Tracey, Cockcroft and Latham, Brozzo and Modified Chaouadi models. Although all these models have been extensively used in the literature (as were previously shown), their predictive capabilities for wire drawing processes in a wide range of reductions have not been specifically addressed. Therefore, the aim of this study is to assess the ability of these models in predicting the initiation of the fracture in the wire (i.e. formation and evolution of the central burst) allowing, for a given die angle, the definition of safe–unsafe reduction operating zones. To this end, tensile tests are firstly carried out to characterize both the hardening parameters and critical damage values for each model. Then, the numerical predictions of the drawing process simulations are compared with available experimental results reported by Orbegozo (1968). In particular, computed drawing forces and damage occurrence are validated. Moreover, relevant model variables such as equivalent strain and triaxility are analyzed to determine their incidence in the formation of central bursts. From these studies, we conclude that triaxiality and deformation play a relevant role in the damage determination. In particular, this aspect is apparent for the highest studied wire reduction, where nonrealistic damage predictions are found. This motivates the proposal of an alternative uncoupled failure criterion combining the effect of deformation and triaxiality. Finally, the performances of all these models in the prediction of fracture initiation in the drawn wires are discussed.

The manuscript is organized as follows. The mechanical formulation including the constitutive and contact models is described in Section ''Mechanical formulation''. Ductile fracture models are detailed in Section ''Fracture models''. Section ''Material characterization via the tensile test'' presents the material characterization via tensile testing. The results of the numerical simulation of the wire drawing process are reported and discussed in Sections ''Numerical simulation of the wire drawing process'' and ''Results and discussion'', respectively. In particular, the new proposed model is presented and assessed in Section ''Distribution of variables along the wire''. Finally, the concluding remarks are summarized in Section ''Conclusions''.

Mechanical formulation

The mechanical formulation used in the present work is based on that proposed by Celentano et al. (2004, 2009) and extended here to incorporate different ductile fracture criteria. A summary of the formulation and the model equations is presented in Table 2.

The mechanical formulation presented above is discretized and solved within the framework of the finite element method according to the numerical approach detailed in Celentano et al. (2004, 2009). Numerical simulations have been run with an in-house code, which have been extensively and successfully used in many forming processes such as multi-pass wire drawing (Celentano et al., 2009), flattening (Celentano and Chaboche, 2007) and many other engineering applications. A new damage sub-routine was implemented into this code to calculate the damage index for each one of the ductile failure models detailed below.

Table 2. Mechanical formulation.

Balance equations			
		Glossary	
Conservation of mass	$\rho J = \rho_0$	ρ	Density
		J	Determinant of the deformation gradient
Conservation of linear momentum	$\nabla \cdot \boldsymbol{\sigma} = 0$	ρ_0	Initial density
		$\boldsymbol{\sigma}$	Cauchy stress tensor
		∇	Spatial gradient operator
Constitutive model			
Stress–strain relationship	$\boldsymbol{\sigma} = \mathbf{C} : (\mathbf{e} - \mathbf{e}^p)$	$\mathbf{C}$	Isotropic elastic constitutive tensor
		$\mathbf{e}$	Almansi strain
Flow rule	$L_v(\mathbf{e}^p) = \dot{\lambda} \frac{\partial F}{\partial \boldsymbol{\sigma}}$	$\mathbf{e}^p$	Plastic component of the strain
		L_v	Lie derivative
		$\dot{\lambda}$	Plastic consistency parameter
Evolution equation of the internal variable $\bar{e}^p$	$\dot{\bar{e}}^p = -\dot{\lambda}$	F	Yield function
		$\dot{\bar{e}}^p$	Effective plastic strain
Yield function	$F = \sigma_{eq} - C - C_{y_0}$	C_{y_0}	Initial yield strength
Von Mises stress	$\sigma_{eq} = \sqrt{3J_2}$	J_2	Second invariant of the deviatoric part of Cauchy stress
		A^p	Hardening coefficient
Isotropic hardening stress	$C = A^p \bar{e}^p n^p$	$\bar{e}^p n^p$	Hardening exponent
Contact and friction model			
Traction vector	$t_{f\,(i)} = -p_n n_{(i)} - a_{(i)} \cdot p_t$		
Normal gap	$g_n = n_{(1)} \cdot (x_{(1)} - x_{(2)})$	p_n,p_t	Normal and tangential pressure
Tangential relative position vector	$g_t = a_{(1)} \cdot (x_{(1)} - x_{(2)})$	x	Spatial coordinate vector
		$n_{(i)}$	Outward unit normal vector
		$a_{(i)}$	Rotation matrix
No contact ($g_n \leq 0$)*:*		E_n,E_t	Normal and tangential stiffness
Normal pressure	$p_n = 0$	g_t^s	Tangential slip vector
Tangential pressure	$p_t = 0$	$\dot{\lambda}_f$	Frictional consistency parameter
Contact ($g_n > 0$)*:*		μ	Friction coefficient
Normal pressure	$p_n = E_n g_n$		
Tangential pressure	$p_t = E_t(g_t - g_t^s)$		
Frictional flow rule	$L_v(g_t^s) = \dot{\lambda}_f \frac{\partial F_f}{\partial p_t}$		
Frictional flow potential	$F_f = \lVert p_t \rVert - \mu p_n$		

Fracture models

As already mentioned, the initiation of ductile damage is evaluated in the present work using the Rice and Tracey, Cockcroft and Latham, Brozzo and Modified Chaouadi models. In order to

Table 3. Ductile fracture models.

Model	Function
Rice and Tracey	$f_1 = 0.283\exp(1.5\xi)$
Cockcroft and Latham	$f_2 = \sigma_1$
Brozzo	$f_3 = \dfrac{2\sigma_1}{3(\sigma_1 - \sigma_h)}$
Modified Chaouadi	$f_4 = \sigma_{eq}\left[1 + 1.461\xi^{\beta}\exp(1.5\xi)\right]$
	$\beta = \begin{cases} 1.25 & \text{for } 0 < \xi < 1 \\ 1.00 & \text{for } 1 > \xi \end{cases}$
New model	$f_5 = \left(\bar{e}^p\right)^{\beta_1}(\xi)^{\beta_2}$

compare their performance, a dimensionless analysis is proposed by means of a fracture index $I_j (j = 1,\ldots,4)$ defined for these four models as (Takuda et al., 1999):

$$I_j = \frac{1}{C_j}\int_0^{\bar{e}^p} f_j \mathrm{d}\bar{e}^p \tag{1}$$

where $C_j = \int_0^{\bar{e}_f^p} f_j \mathrm{d}\bar{e}^p$ C_j is the critical damage, $\bar{e}_f^p$ is the effective plastic deformation at the fracture stage and f_j is a function expressed for each model as detailed in Table 3. Here, σ_1 is the maximum principal stress, σ_h is the hydrostatic pressure (defined as 1/3 of the trace of σ) and $\xi = \sigma_h/\sigma_{eq}$ is the triaxiality. It is seen that, regardless of the model used, the fracture condition starts when $I_j \geq 1$. It is assumed that both $\bar{e}_f^p$ and C_j are characteristic material parameters that can be derived, as shown in Section ''Ductile fracture models'', from tensile tests.

In addition to these four classical models, a new criterion which exponentially weighs the effects of triaxiality and effective plastic deformation is also presented in Table 3. As already mentioned in Section ''Introduction'', these two parameters have great relevance in the fracture process and also in wire drawing processes (Celentano et al., 2009). In this new criterion, β_1 is the plastic deformation exponent and β_2 is the triaxiality exponent, both dependent on the material.

Material characterization via the tensile test

Hardening response

As described in Celentano et al. (2004), the characterization of the hardening response of a material can be accomplished through the numerical simulation of the tensile test applying the mechanical formulation described in Section ''Mechanical formulation''. In this context, the hardening parameters were obtained from the least-squares fitting of the numerical tensile true stress–strain curve to the corresponding experimental Al-2011 aluminum alloy measurements reported by Orbegozo (1968).

Figure 2 shows the experimental curve together with the numerical fitting applying this procedure. The resulting material parameters are summarized in Table 4.

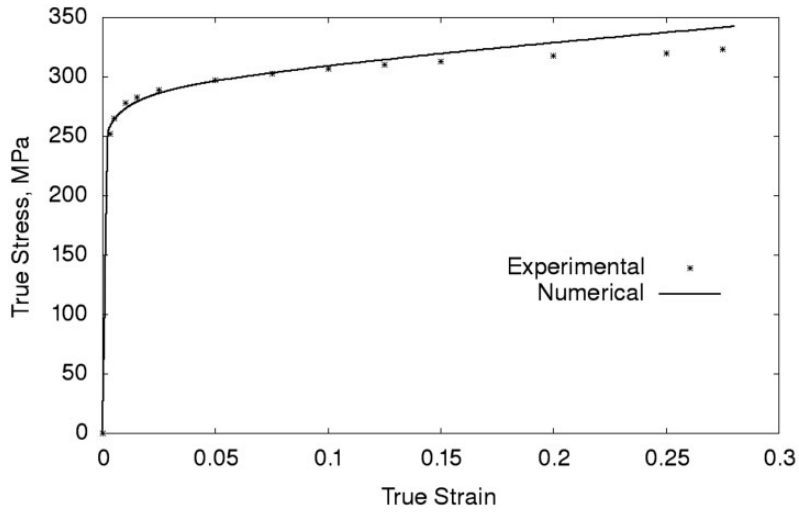

Figure 2. Experimental (Orbegozo, 1968) and numerical tensile true stress–strain curves of the Al-2011 aluminum alloy.

Table 4. Mechanical parameters of the Al-2011 aluminum alloy.

Parameter	Value
Density	2830 kg/m^3
Young's modulus	75,652 MPa
Poisson's ratio	0.33
Yield strength	251.9 MPa
Hardening coefficient	344.7 MPa
Hardening exponent	0.05

Ductile fracture models

To characterize the five damage models presented in Section "Fracture models", the numerical simulation of the tensile test described in Section "Hardening response" was also used in order to obtain the critical values for each model. First of all, the true strain is calculated as $ln\left(A_0/A\right)$, A_0 and A being the respective initial and deformed transversal areas of the specimen at the necking zone. When this deformation reaches the experimentally measured failure strain (approximately 0.28 as can be seen in Figure 2), it is assumed that the fracture process starts. The damage value obtained at this time in the necking zone is assumed as the critical value. This value has to be computed for each of the five models presented above. The values obtained from this numerical characterization are presented in Table 5. For the new model, $\beta_1 = 0.2$ and $\beta_2 = 1.7$ were considered.

Table 5. Computed critical damage values.

Model	Constant	Value
Rice and Tracey	C_1	0.169
Cockcroft and Latham	C_2	106.81 MPa
Brozzo	C_3	0.343
Modified Chaouadi	C_4	195.62 MPa
New model	C_5	0.057

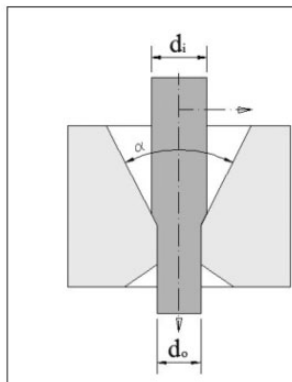

Single-pass geometries

Red (%)	Angle α (°)	di (mm)	do (mm)
5	30	5.90	5.74
9	30	6.02	5.74
18	30	6.34	5.74
25	30	6.62	5.74
33	30	6.70	5.74
39	30	7.34	5.74

Figure 3. Wire drawing: geometry of the wire and die.

Numerical simulation of the wire drawing process

Geometric configuration

The geometry of the cases studied here is detailed in Figure 3. As reported by Orbegozo (1968), these cases were experimentally carried out using Al-2011 aluminum alloy wires drawn in a single pass configuration keeping the die angle constant (30°) and changing gradually the reduction levels of the wire. This was achieved by varying only the input diameter (d_i) using a constant output diameter ($d_o = 5.74$ mm) determined by the drawing die. The reductions under which the drawn material presented central burst were also specified.

Finite element model

Figure 4 shows the axisymmetric spatial discretization used in this work for the numerical simulation of the drawing process. Four-noded isoparametric elements were used for the wires. The drawing die was assumed to be rigid, and its discretization was made by means of two-noded isoparametric elements. The size of the final used mesh was chosen after a sensitivity analysis to ensure obtaining good quality results. The threading zone (conical reduction of the wire) was only considered to allow part of the wire to pass through the drawing die in order to be able to apply the drawing force. The use of a coarser mesh in this zone does not affect the quality of the results obtained on the wire.

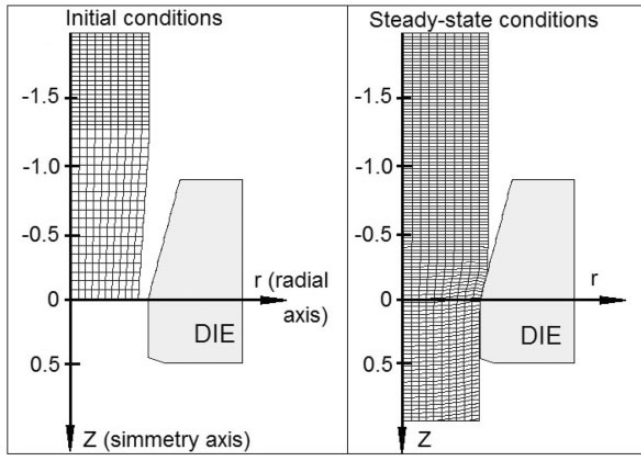

Spatial discretization	
Wire	2000 four noded isoparametric elements
Die	200 two noded isoparametric elements
Contact	61 two noded isoparametric elements
Time discretization	
Number of time steps	500
Boundary conditions	
Prescribed displacement	0.04 m
Fricction coefficient	0.1
Normal rigidity	0.5E+08 MPa/m
Tangential rigidity	0.5E+06 MPa/m

Figure 4. Wire drawing: spatial discretization.

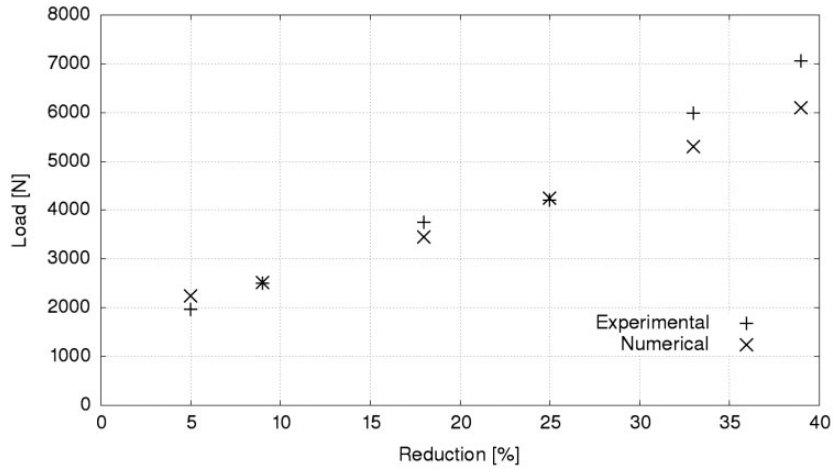

Figure 5. Drawing forces.

All simulations were carried out using a time-dependent linear displacement imposed at the bottom zone of the wire in order to obtain a constant and low drawing speed of $v_d = 9.6\,\text{mm/min}$. Celentano et al. (2009) and Celentano (2010) have shown that low drawing velocities do not induce rate dependent effects on the material response and, therefore, they have no incidence on the development of ductile fracture in these situations.

The friction coefficient was chosen on the basis to obtain, as shown below, realistic predictions of the wire drawing force for the cases summarized in Figure 5. Moreover, as suggested by Green and Hill (1952), the hydrostatic pressure should not vary significantly for low values of friction coefficient as the one chosen in the present analysis.

Results and discussion

Drawing forces

To validate the numerical models studied, the steady-state forces obtained from the present numerical simulations were compared with those reported experimentally by Orbegozo (1968). Figure 5 shows the forces for each of the six reductions presented in Figure 3. It is seen that for the smaller four reductions, the model reproduces well the values of the drawing forces, and only in the last two reductions there is a bigger difference between the experimental and computed values.

Experimental error ranges were not reported for the obtained forces. Even so, numerical values do not exceed 12%, thus validating the numerical results.

Damage

The computed steady-state damage results are summarized in Figure 6, where the maximum damage indexes reached for the four classical models analyzed (R and T: Rice and Tracey model; C and L: Cockcroft and Latham model; Ch.mod.: Modified Chaouadi model) together with the results obtained with the proposed new model are reported in the wire axis for each of the six reductions studied. Moreover, the graph shows the safe (white area) and unsafe zones (gray area) according to the experimental results reported by Orbegozo (1968).

It is seen that the Rice and Tracey model, which was originally defined as a criterion that considers the influence of the triaxiality of the stress field on the evolution of cavities, provides an acceptable description of the failure occurrence. Nevertheless the damage is respectively underestimated and overestimated for the reductions of 18% and 39%. Moreover, the Cockcroft and Latham model underestimates the level of damage in the cases with reduction of 18% and 25%.

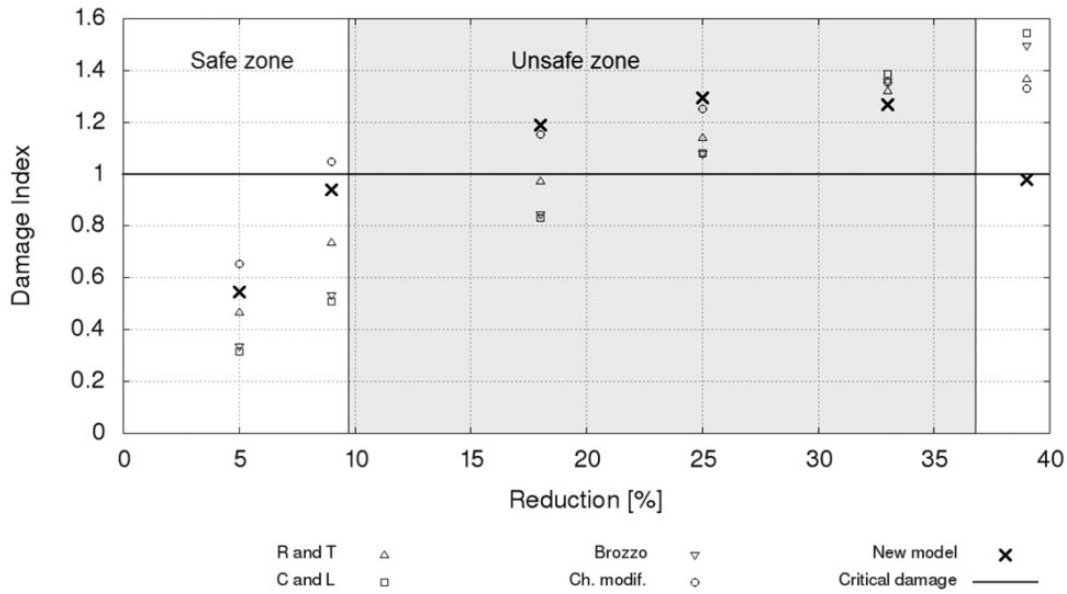

Figure 6. Damage index values.

The initiation of central bursts in the axis of the wire is wrongly predicted since this criterion only considers the principal maximum stress and does not account for the effect of the triaxiality presented in the contact zone of the wire with the drawing die. This model also shows an increasing trend in the damage level when the reduction level increases but it does not succeed in reproducing the decrease of the damage index experimentally reported for the largest reduction (39%). On the other hand, the Brozzo model, which behaves very similarly to the Cockcroft and Latham model, is not able to represent the desired phenomenon because although it incorporates the effect of hydrostatic pressure in the damage criterion, it does not consider the relation between pressure and the Von Mises stress. Modified Chaouadi model is, among the four classical models studied, the one that best reproduces the phenomenon of the beginning of chevron formation in drawn wires. This criterion succeeds in predicting correctly the beginning of fracture in the wire. This model slightly overestimates the damage prediction for the greater reduction (39%), but satisfactorily reproduces the drop in the value of the obtained damage.

The damage indexes obtained with the new model are also included in Figure 6 where an improved performance of the proposed criterion can clearly be seen. In particular, the damage index for the highest reduction (39%) not only decreases but also falls below the threshold of critical damage, entering into the safe zone mainly due to the sharp drop in the value of the triaxiality.

Distribution of variables along the wire

To have a better understanding of the behavior of each model, the evolutions of some specific variables that have an incidence on the beginning of fracture are analyzed on a node located on the axis of the wire. To be able to compare the six geometric configurations presented, an axial nondimensionalization is proposed as a function of the incoming diameter of the wire. The numerical simulations show that the results at an incoming diameter behind the beginning of the calibration zone and at an incoming diameter after the same point do not present significant variations. Therefore, the study is centered in this range ($[-d_i:d_i]$), whose adimensionalization falls within the range of [−1:1] as shown in Figure 4.

Figure 7 presents the axial distributions of von Mises stress, hydrostatic pressure and maximum principal stress (all of them on the left side axis), and the effective plastic deformation (on the right side axis), for four of the six reductions studied. The damage index (left side axis) and triaxiality (right side axis) evolutions are also shown.

It is appreciated that the damage evolves only under positive values of hydrostatic pressure. No damage evolution is observed under negative hydrostatic pressures, since the microcavities would tend to close under compressive states. On the other hand, the beginning and later evolution of damage takes place in the same range in which the effective plastic deformation starts and grows since, as it is well known, ductile fracture is characterized by having high levels of plastic deformation. These curves also show that the damage evolution mainly occurs when the wire contacts the drawing die. Once the wire enters the calibration zone (the cylindrical zone of the drawing die), the damage evolution stops.

Figure 8 reports the steady-state contour maps of the variables for four characteristic reductions (the same as those analyzed in Figure 7). When the reduction increases, the effective plastic deformation in the wire surface increases and, at the same time, propagates strongly towards the center of the wire. For small reductions, a positive hydrostatic pressure peak appears on the center of the wire, which decreases while the reduction increases because the contact area between the wire and die grows and the compression propagates to the center. This effect is mainly responsible for the

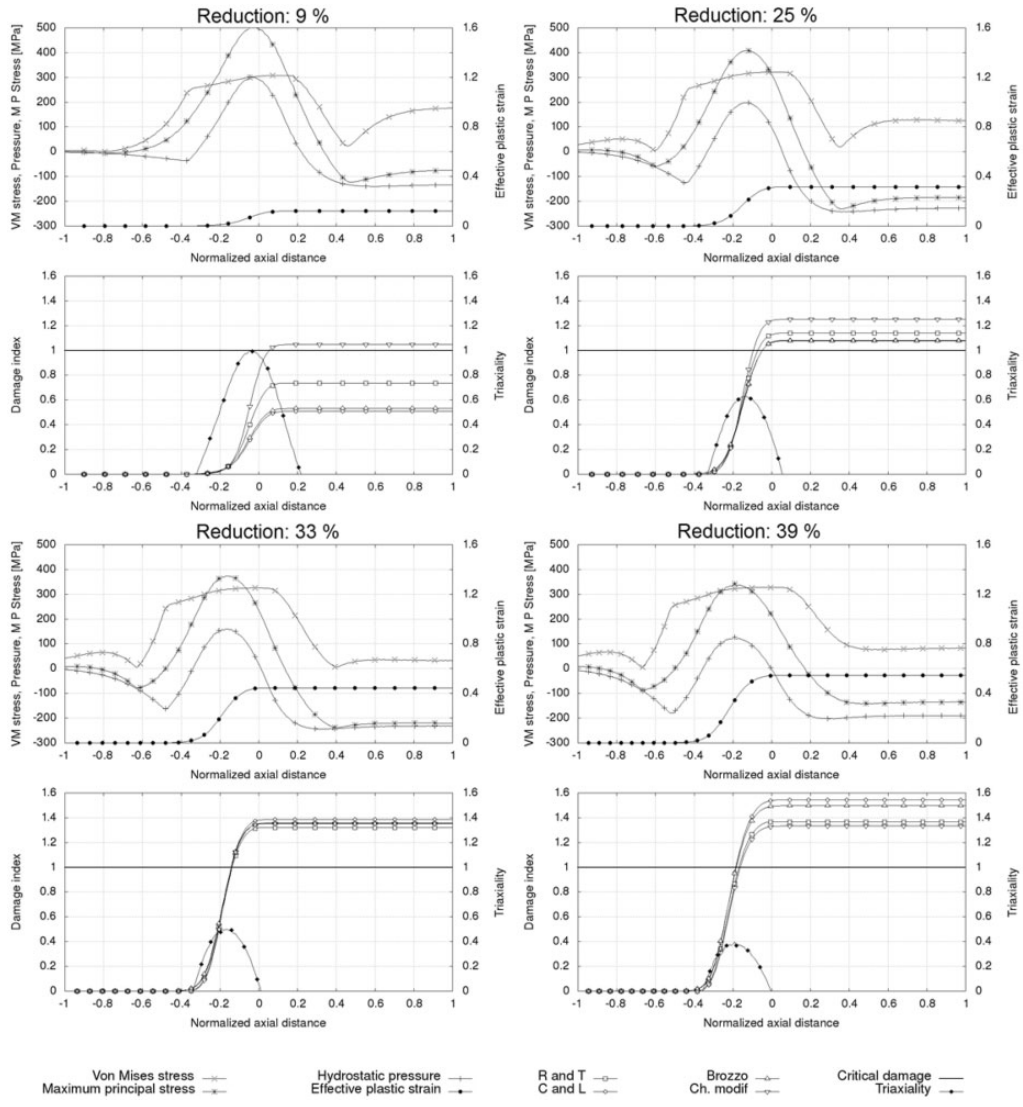

Figure 7. Axial distributions of Von Mises Stress, hydrostatic pressure, maximum principal stress, effective plastic deformation, triaxiality and damage index for each of the five ductile failure models, for four reductions (9%, 25%, 33% and 39%).

decrease of the triaxiality. Finally, the von Mises stress has a similar trend along all reductions, slightly increasing its value when the reduction increases.

Rice and Tracey model. This criterion has a strong dependence on triaxiality but only in the exponent of the function as shown in Table 3. Therefore, the decrease of the triaxiality observed in Figure 7 is not enough to cause a decrease in the damage index.

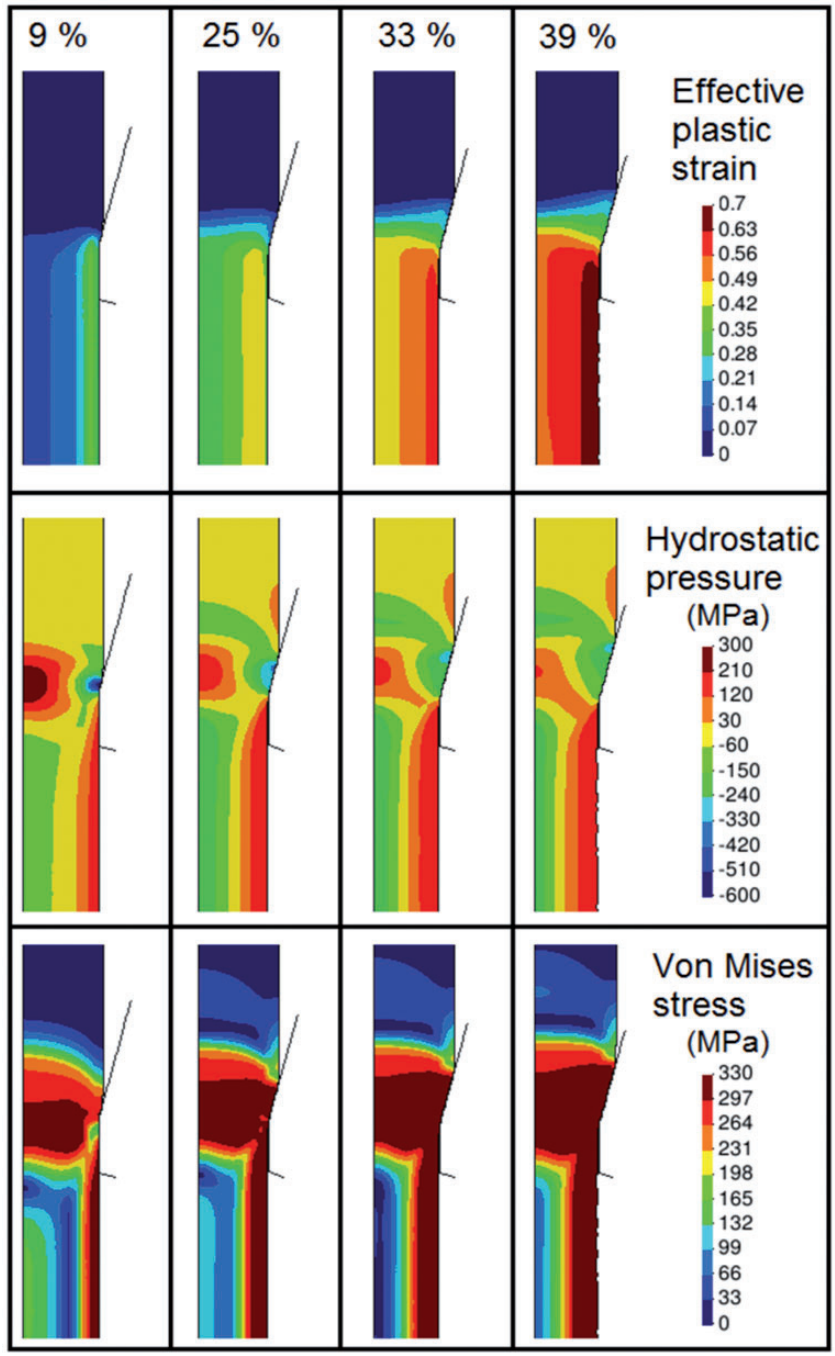

Figure 8. Contours of effective plastic deformation, hydrostatic pressure and von Mises stress for four reductions (9%, 25%, 33% and 39%).

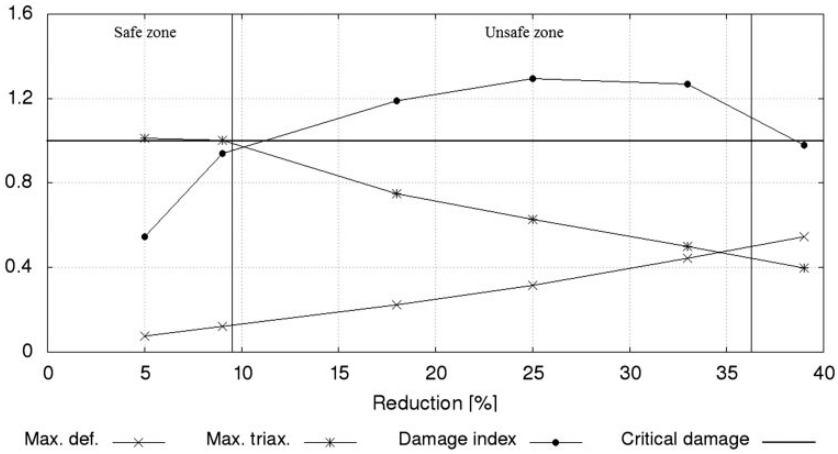

Figure 9. Maximum plastic deformation, maximum triaxiality and damage index of the new model.

Cockcroft and Latham model. This criterion only considers the maximum principal stress evaluated under the integral of the plastic deformation as it can be seen in Table 3. Figure 7 shows a decrease of σ_1 but a strong increase in the plastic effective deformation in the center of the wire, promoting an increasing trend of the damage index.

Brozzo model. In contrast to the Cockcroft and Latham criterion, this model incorporates the effect of the equivalent stress but, as it was shown above, this effect is not significant. This causes that the trends exhibited by the Brozzo and Cockcroft and Latham models are very similar.

Modified Chaouadi model. In contrast to the Rice and Tracey model, this criterion emphasizes the role of the triaxility thus leading to a decrease of the damage index for the greatest reductions where the triaxiality is lower. Although this criterion is unable to provide a damage index below the critical limit for the reduction of 39%, it is the only one that presents a slightly decreasing trend.

New model. The distributions of variables along the wire show that the damage strongly depends on the effective plastic deformation and triaxiality. This is the reason why such variables were considered in the proposed criterion in order to achieve more realistic damage predictions that adequately agree with the experimental results. Figure 9 correlates both variables (maximum plastic deformation and maximum triaxiality achieved in the center of the wire) with the damage index, where increasing and decreasing trends of plastic deformation and triaxiality can be respectively observed for greater levels of wire reductions. Lower reductions (5% and 9%) present low values of plastic deformation but high values of triaxiality (even so, no evidence of internal damage was found). By increasing the reduction (18%, 25% and 33%), plastic deformation grows and triaxiality decreases (in these cases, the fracture condition is reached). Finally, the last reduction (39%) presents high levels of plastic deformation in the center of the wire but low values of triaxiality (no evidence of fracture was found under this configuration). All in all, the proposed model weighs both variables, assigning a low exponent to the plastic deformation and a high exponent to the triaxiality. Thus, all the experimental results presented by Orbegozo are properly reproduced.

Conclusions

A comparative study including four well-known ductile fracture models (i.e. the Rice and Tracey, Cockcroft and Latham, Brozzo and Modified Chaouadi models) together with a proposed criterion has been presented. The study is focused on an Al-2011 aluminum alloy single-pass wire drawing process. Six different reductions have been analyzed with the aim to compare the numerical predictions with experiments available in the literature. To this end, a large strain elastoplastic formulation was applied to describe the evolution of stresses and deformation. The numerical simulations report a very good agreement with the experimental drawing forces. Moreover, the damage was computed using the mentioned ductile fracture models. Although reasonable damage predictions can be obtained with the four analyzed classical models, they were not able to accurately reproduce the experimental data for all the studied wire reductions. In particular, the Modified Chaouadi model was the only one able to reduce the damage in the greatest reduction, showing the strong relationship between the damage evolution and triaxiality. On the other hand, the new ductile fracture model was found to satisfactorily predict the beginning of the central bursts thus exhibiting a good damage description for all reductions.

Future research will be devoted to the assessment of coupled damage models (e.g. Lemaitre and Gurson models) in their predictive capabilities to describe fracture initiation of different materials subjected to single and multi-pass wire drawing processes.

Declaration of conflicting interests

The author(s) declared no potential conflicts of interest with respect to the research, authorship, and/or publication of this article.

Funding

The author(s) disclosed receipt of the following financial support for the research, authorship, and/or publication of this article: The support provided by the Chilean Council of Research and Technology CONICYT (FONDECYT Project 1130404) and the Scientific Research Projects Management Department of the Vice Presidency of Research, Development and Innovation (DICYT-VRID) at Universidad de Santiago de Chile, Proyecto Basal USA1555 are gratefully acknowledged.

References

Avitzur B (1983) *Handbook of Metal-Forming Processes*. New York, USA: John Wiley and Sons.

Brozzo P, De Luca B and Redina R (1972) A new method for the prediction of the formability limits of metal sheets. *Proceedings of the seventh biannual conference of the international deep drawing research group*.

Celentano D, Cabezas E, García C, et al. (2004) Characterization of the mechanical behaviour of materials in the tensile test: Experiments and simulation. *Modelling and Simulation in Materials Science and Engineering* 12: 425–444.

Celentano D and Chaboche JL (2007) Experimental and numerical characterization of damage evolution in steels. *International Journal of Plasticity* 23: 1739–1762.

Celentano DJ, Palacios MA, Rojas EL, et al. (2009) Simulation and experimental validation of multiple-step wire drawing processes. *Finite Elements in Analysis and Design* 45: 163–180.

Celentano DJ (2010) Thermomechanical simulation and experimental validation of wire drawing processes. *Materials and Manufacturing Processes* 25: 546–556.

Chaouadi R, De Meester P and Vandermeulen W (1994) Damage work as ductile fracture criterion. *International Journal of Fracture* 66: 155–164.

Choi JS, Lee HC and Im YT (2010) A study on chevron crack formation and evolution in a cold extrusion. *Journal of Mechanical Science and Technology* 24(9): 1885–1890.

Cockcroft M and Latham D (1968) Ductility and workability of metals. *Journal of Institute of Metals* 96: 33–39.

Freudenthal AM (1950) *The Inelastic Behaviour of Engineering Materials and Structures*. New York, USA: John Wiley and Sons.

Green AP and Hill R (1952) Calculations on the influence of friction and die geometry in sheet drawing. *Journal of the Mechanics and Physics of Solids* 1: 31–36.

Gurson AL (1977) Continuum theory of ductile rupture by void nucleation and growth: Part I – Yield criteria and flow rules for porous ductile media. *Journal of Engineering Materials and Technology* 99(1): 2–15.

Haddi A, Imad A and Vega G (2012) The influence of the drawing parameters and temperature rise on the prediction of chevron crack formation in wire drawing. *International Journal of Fracture* 176: 171–180.

Huang Y (1991) Accurate dilatation rate for spherical voids in triaxial stress fields. *ASME Journal of Applied Mechanics* 58: 1084–1086.

Ko D and Kim B (2000) The prediction of central burst defects in extrusion and wire drawing. *Journal of Materials Processing Technology* 102: 19–24.

Komori K (2003) Effect of ductile fracture criteria on chevron crack formation and evolution in drawing. *International Journal of Mechanical Sciences* 45: 141–160.

Lemaitre J (1985) A continuous damage mechanics model for ductile fracture. *Journal of Engineering Materials and Technology* 107: 83–89.

McAllen P and Phelan P (2005) Ductile fracture by central bursts in drawn 2011 aluminium wire. *International Journal of Fracture* 135: 19–33.

McAllen P and Phelan P (2007) Numerical analysis of axisymmetric wire drawing by means of a coupled damage model. *Journal of Materials Processing Technology* 183: 210–218.

McClintock FA (1968) Local criteria for ductile fracture. *International Journal of Fracture Mechanics* 4(2): 101–130.

Norasethasopon S and Yoshida K (2008) Prediction of chevron crack initiation in inclusion cooper shaped-wire drawing. *Engineering Failure Analysis* 15: 378–393.

Orbegozo JI (1968) Fracture in wire drawing. *Annals of the CIRP* 16: 319–330.

Pardoen T, Delatte P, Morhet J, et al. (1996) Application of local damage and fracture models to notched round copper bars. *Journal de Physique* 6: 145–153.

Ran JQ and Fu MW (2016) Applicability of the uncoupled ductile fracture criteria in micro-scaled plastic deformation. *International Journal of Damage Mechanics* 25(3): 289–314.

Rice JR and Tracey DM (1969) On ductile enlargement of voids in triaxial stress fields. *Journal of Mechanical Physics of Solids* 17: 210–217.

Sowerby R, Chandrasekaran N, Dung NL, et al. (1985) The prediction of damage accumulation during upsetting tests based on McClintock's model. *Forschungim Ingenieurwesen* 51(5): 147–150.

Takuda H, Mori K and Hatta N (1999) The application of some criteria for ductile fracture to the prediction of the forming limit of sheet metals. *Journal of Materials Processing Technology* 95: 116–121.